Available online at www.sciencedirect.com
ScienceDirect
Journal of the European Ceramic Society 29 (2009) 2831–2839
www.elsevier.com/locate/jeurceramsoc

# Sintering behaviour of $La_{1-x}Sr_xCo_{0.2}Fe_{0.8}O_{3-\delta}$ ($0.3 \leq x \leq 0.8$) mixed conducting materials

A. Möbius *, D. Henriques, T. Markus

*Forschungszentrum Jülich GmbH, Institute of Energy Research, 52425 Jülich, Germany*

Received 11 February 2009; received in revised form 31 March 2009; accepted 2 April 2009
Available online 7 May 2009

**Abstract**

The sintering behaviour of different materials within the system $La_{1-x}Sr_xCo_{0.2}Fe_{0.8}O_{3-\delta}$($0.3 \leq x \leq 0.8$) was investigated. Shrinkage curves were measured up to 1350 °C using a vertical high-resolution dilatometer. The measurements showed that the influence of the heating rate on the shrinkage curves is negligible. Furthermore, the relative shrinkage increases with decreasing lanthanum content in the perovskite lattice at a constant sintering temperature. Sintering experiments showed that the influence of the sintering temperature on the microstructure and densification is more significant than the influence of the dwell time. Increasing the sintering temperature led to a higher densification even at low sintering dwell times. There seems to be no influence of the lanthanum content on the final sintering temperature and dwell time. Nevertheless, sintering at the highest sintering temperature led to the formation of cobalt oxide in case of $La_{0.6}Sr_{0.4}Co_{0.2}Fe_{0.8}O_{3-\delta}$ and $La_{0.7}Sr_{0.3}Co_{0.2}Fe_{0.8}O_{3-\delta}$.


*Keywords:* Sintering behaviour; LSCF; MIEC; Oxyfuel

## 1. Introduction

In the oxyfuel combustion process the fossil fuel is combusted with pure oxygen. Due to the combustion of the fossil fuel with pure oxygen the exhaust gas is highly concentrated in $CO_2$ which could be separated and then stored. In recent years gas separation membranes are considered to be an efficient technology for the future generation of zero $CO_2$-emission power plants. Gas separation membranes seem to be a less energy consumptive approach in comparison to cryogenic air decomposition to produce pure oxygen.

Perovskite-type, mixed ionic and electronic conducting (MIEC) materials within the system $La_{1-x}Sr_xCo_{1-y}Fe_yO_{3-\delta}$ (LSCF) have received great interest concerning their ability to separate oxygen from air. Furthermore, those materials could be used for partial oxidation of methane and as well as electrodes in solid oxide fuel cells (SOFC).[1–3]

Perovskite-type materials within the system $La_{1-x}Sr_xCo_{1-y}Fe_yO_{3-\delta}$could be used as gas separation membranes. Therefore, it is necessary to produce dense membranes (> 90% of the theoretical density).[4] It is known from research studies on MIEC membrane materials that those LSCF materials swell if the sintering temperature is too high.[5,6] Hence, preferably optimal sintering conditions for those perovskite-type materials are essential. The sintering behaviour of LSCF materials has to our knowledge not been studied systematically. In this study the sintering behaviour of $La_{1-x}Sr_xCo_{0.2}Fe_{0.8}O_{3-\delta}$($0.3 \leq x \leq 0.8$) is investigated. Hence, shrinkage curves have been measured and sintering experiments under different conditions have been conducted. The microstructure of the sintered samples was investigated by scanning electron microscopy (SEM). The density of the sintered samples was measured using the Archimedes method.

## 2. Experimental

$La_{1-x}Sr_xCo_{0.2}Fe_{0.8}O_{3-\delta}$($0.3 \leq x \leq 0.8$) compositions are designated by the abbreviation LSCF. Numerals following the abbreviation refer to the relative molar proportions of each cation. For example, $La_{0.3}Sr_{0.7}Co_{0.2}Fe_{0.8}O_{3-\delta}$ is designated as LSCF3728.

* Correspondingauthor. Tel.: +49 2461615870; fax: +49 2461613699.
*E-mail address:* a.moebius@fz-juelich.de (A. Möbius).

0955-2219/$ – see front matter © 2009 Elsevier Ltd. All rights reserved.
doi:10.1016/j.jeurceramsoc.2009.04.003

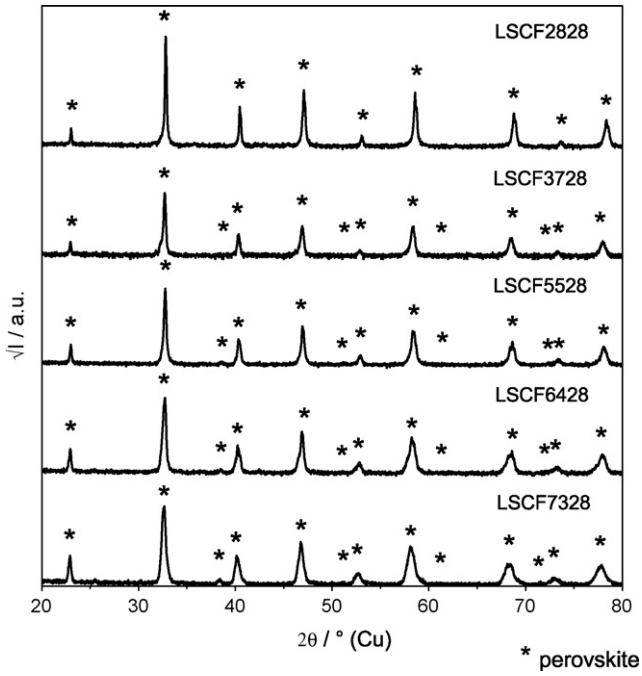


Fig. 1. XRD pattern of the as-calcined powders.

### 2.1. Sample preparation

Perovskite-type powders were prepared by solid state reaction. Thereto, $La_2O_3$, $SrCO_3$, $CoCO_3$ and $Fe_2O_3$ were mixed in appropriate proportions and calcined in air at 1150 °C for 6–24 h. The calcination temperature was determined by differential thermal analysis (DTA) of the stoichiometrically mixed powders up to 1200 °C using a STA 449C Jupiter (Netzsch, Germany).

The calcined powders were first ground in a mortar and then ball milled for 24 h in ethanol. The final powders were uniaxially pressed into pills (8 mm in diameter, 4–5 mm in height, 125 MPa pressure).

### 2.2. Characterisation of as-calcined powders

All materials were single-phase according to XRD (X-ray diffraction) measurements using a D8 Advance Series 2 (Bruker AXS, Germany). The XRD patterns are shown in Fig. 1.

The perovskite phase was identified using appropriate powder diffraction files (JCPDS-database). The calcined powders had an average particle size $d_{50}$ of approximately 0.5 μm. The particle size distribution was measured by laser diffraction (Laser Particle Sizer ANALYSETTE 22, Fritsch, Germany). The chemical composition of the as-prepared materials was checked using inductively coupled plasma optical emission spectrometry (ICP-OES, IRIS Intrepid, TJA, USA). The chemical and physical properties are summarised in Table 1.

### 2.3. Dilatometry

Shrinkage curves of the pressed pills were measured using a vertical high-resolution dilatometer (TMA Setsys Evolution, Setaram, France). Using this dilatometer dimension changes as small as 0.01 μm are detectable with a resolution of 0.2 nm. The samples were heated up to the final temperature, which was in the range of 1050–1350 °C. All measurements were conducted in air using a load of 5 g.

The relative shrinkage $\varepsilon$ was calculated on the basis of the instantaneous elongation $\Delta L$ and the length of the green body $L_0$:

$$\varepsilon = \frac{\Delta L}{L_0} \times 100\% \quad (1)$$

In addition the shrinkage rate was calculated:

$$\frac{\Delta \varepsilon}{\Delta t} \quad (2)$$

### 2.4. Archimedes method

The density of the sintered samples was measured by the Archimedes method in water. The theoretical density $\rho_{theo}$ was calculated from the lattice parameters:

$$\rho_{theo} = \frac{M_{perovskite} \cdot Z}{N_A \cdot V_{UC}} \quad (3)$$

where $M_{perovskite}$, $Z$, $N_A$ and $V_{UC}$ are the molar mass of the perovskite, the number of units, the Avogadro constant and the volume of the unit cell, respectively. The volume of the unit cell is calculated from the lattice parameters. For the calculation of the molar mass of the perovskite, the oxygen stoichiometry was assumed to be 3.0.

The relative density is the ratio of the sample density to the theoretical density.

### 2.5. Scanning electron microscopy

The microstructure of the samples was investigated using scanning electron microscopy (SEM). Thereto, the samples were embedded in epoxy resin, ground and polished to create cross-sections. SEM investigations were conducted using a LEO440

Table 1
Chemical and physical properties of the as-calcined powders.

| | Chemical composition | $d_{50}$ (μm) | Secondary phases | $V_{UC}$ (cm$^3$) | $Z$ | $\rho_{theo}$ (kg/m$^3$) |
|---|---|---|---|---|---|---|
| LSCF2828 | $La_{0.2}Sr_{0.8}Co_{0.2}Fe_{0.8}O_{3-\delta}$ | 0.44 | None | $5.7030 \times 10^{-23}$ | 1 | 5.89 |
| LSCF3728 | $La_{0.3}Sr_{0.7}Co_{0.2}Fe_{0.8}O_{3-\delta}$ | 0.62 | None | $3.4913 \times 10^{-22}$ | 6 | 5.92 |
| LSCF5528 | $La_{0.5}Sr_{0.5}Co_{0.2}Fe_{0.8}O_{3-\delta}$ | 0.45 | None | $3.4805 \times 10^{-22}$ | 6 | 6.23 |
| LSCF6428 | $La_{0.6}Sr_{0.4}Co_{0.2}Fe_{0.8}O_{3-\delta}$ | 0.57 | None | $3.4920 \times 10^{-22}$ | 6 | 6.36 |
| LSCF7328 | $La_{0.7}Sr_{0.3}Co_{0.2}Fe_{0.8}O_{3-\delta}$ | 0.56 | None | $3.5193 \times 10^{-22}$ | 6 | 6.45 |

Stereoscan (Carl Zeiss NTS GmbH, Germany) and an acceleration voltage of 20 kV.

For phase investigations an energy dispersive X-ray (EDX) detector was used (Si(Li)-detector, Oxford Instruments, UK).

## 3. Results and discussion

### 3.1. Effect of heating rate on shrinkage curves

The influence of the heating rate on the shrinkage curves was investigated by measuring shrinkage curves using heating rates of 2 °C/min, 6 °C/min and 10 °C/min at temperatures between 800 °C and 1200 °C, 1300 °C and 1350 °C, respectively. The samples were dwelled at the final temperature for 30 min. To assure solid state sintering DTA measurements up to 1550 °C were conducted to determine the solidus temperature of the perovskites.

The shrinkage curves depending on the heating rate are shown in Fig. 2. There seemed to be an influence of the heating rate on the shrinkage curve in case of LSCF2828 (Fig. 2a), LSCF3728 (Fig. 2b) and LSCF6428 (Fig. 2d). In case of LSCF5528 (Fig. 2c) the heating rate influenced the shrinkage curves at temperatures higher than 1200 °C. The sintering experiments using LSCF7328 (Fig. 2e) showed that the heating rate had almost

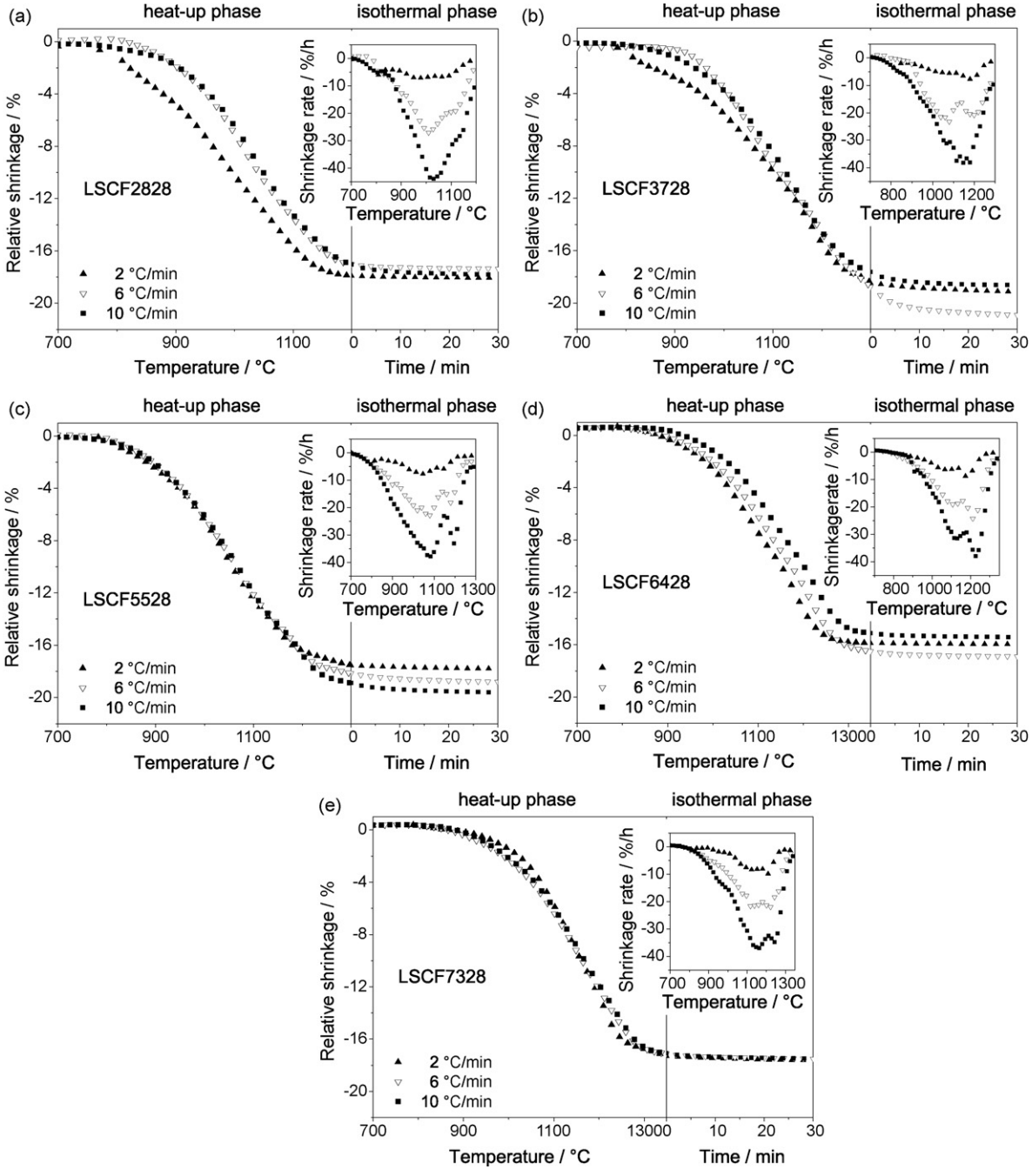


Fig. 2. Relative shrinkage vs. temperature and time and shrinkage rate vs. temperature of different LSCF samples depending on heating rate.

Table 2
Selected sintering temperatures.

| | $T_1$ (°C) | $T_2$ (°C) | $T_3$ (°C) |
|---|---|---|---|
| LSCF2828 | 950 | 1050 | 1150 |
| LSCF3728 | 950 | 1050 | 1250 |
| LSCF5528 | 950 | 1050 | 1150 |
| LSCF6428 | 1050 | 1150 | 1250 |
| LSCF7328 | 1050 | 1150 | 1250 |

no influence on the shrinkage curves in the range of those investigations. Here, deviations were within the uncertainty of the measurement. The total shrinkage was in all cases less than 25%.

### 3.2. Determination of sintering temperature

Suitable sintering temperatures can be derived from shrinkage rate curves. Minima in shrinkage rate curves indicate a change in transport mechanism. Therefore, it is important to investigate the sintering behaviour below a minimum and at a minimum of the shrinkage rate curve.

The shrinkage rate curves depending on the heating rate are shown in Fig. 2(embedded graphs). According to the shrinkage rate curves, a temperature below the first ($T_1$), in the range of the first ($T_2$) and in the range of the second minimum of the shrinkage rate curve ($T_3$) were chosen as sintering temperatures for futher investigations (Table 2).

### 3.3. Effect of sintering temperature on shrinkage curves and sample density

Samples were heated up to 800 °C using a heating rate of 10 °C/min; between 800 °C and 1000 °C with a heating rate of 6 °C/min, and between 1000 °C and the final sintering temperature 2 °C/min. All samples were dwelled at the final temperature for 6 h.

In Fig. 3 the measured shrinkage curves depending on the sintering temperature are shown. The measured relative sample densities are summarised in Table 3.

Preliminary sintering experiments for LSCF2828, LSCF3728 and LSCF5528 showed that sintering at $T_1 = 950$ °C (temperature below the first minimum of shrinkage rate curve) led to a comparatively low densification. Thus, no shrinkage curves were measured at this temperature.

In case of LSCF6428 and LSCF7328 sintering experiments at a temperature below the first minimum of the shrinkage rate curve ($T_1$) showed that the densification is not completed (Fig. 3a). This can be seen in the isothermal phase of the shrinkage curves. In this phase the shrinkage did not reach a constant level after 6 h dwelling. Here, the total shrinkage was ≈ 5% for LSCF6428 and ≈ 9% for LSCF7328. The measured relative densities using Archimedes method were between ≈ 81% and ≈ 86% of the theoretical density.

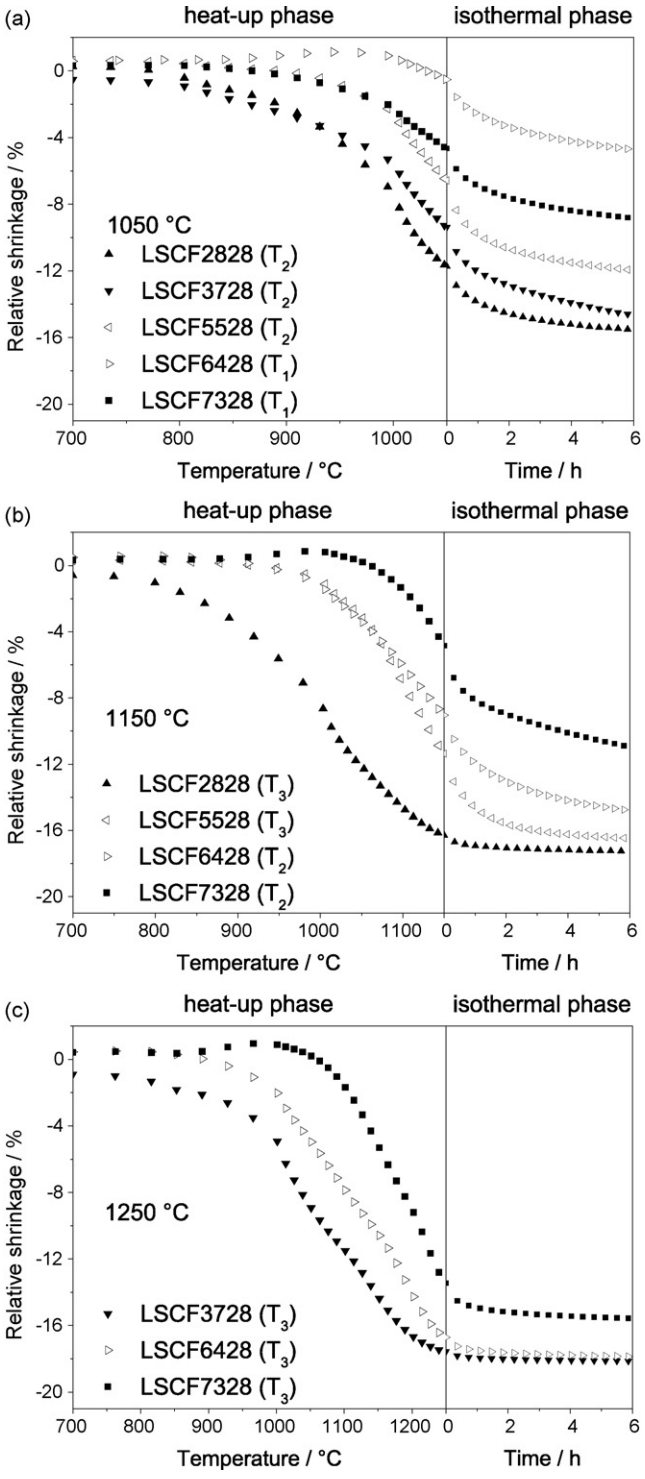


Fig. 3. Relative shrinkage vs. temperature and time of different LSCF samples depending on sintering temperature.

Table 3
Measured relative sample densities depending on sintering temperature.

| | 1050 °C | 1150 °C | 1250 °C |
|---|---|---|---|
| LSCF2828 | ≈ 94% | > 95% | – |
| LSCF3728 | ≈ 92% | – | > 95% |
| LSCF5528 | ≈ 89% | > 95% | – |
| LSCF6428 | ≈ 81% | ≈ 94% | > 95% |
| LSCF7328 | ≈ 86% | ≈ 93% | > 95% |

By sintering at a temperature in the range of the first minimum of the shrinkage rate curve ($T_2$) the densification is also not

Table 4
Measured relative sample densities depending on sintering temperature and dwell time (* cracks in sample).

| | 1050 °C | | | 1150 °C | | | 1250 °C | | |
|---|---|---|---|---|---|---|---|---|---|
| | 0.5 h | 3 h | 6 h | 0.5 h | 3 h | 6 h | 0.5 h | 3 h | 6 h |
| LSCF2828 | ≈ 88% | ≈ 92% | ≈ 94% | ≈ 93% | ≈ 93% | ≈ 93% | – | – | – |
| LSCF3728 | ≈ 84% | ≈ 92% | ≈ 93% | – | – | – | > 95% | > 95% | > 95% |
| LSCF5528 | ≈ 86% | ≈ 83% | ≈ 91% | ≈ 94% | ≈ 94% | ≈ 95% | – | – | – |
| LSCF6428 | ≈ 61% | ≈ 81% | ≈ 66%* | ≈ 80% | ≈ 88% | ≈ 80%* | ≈ 87% | ≈ 89% | ≈ 95% |
| LSCF7328 | ≈ 80% | ≈ 83% | ≈ 85% | ≈ 94% | > 95% | > 95% | > 95% | > 95% | > 95% |

completed after dwelling for 6 h, but higher than in case of a lower sintering temperature. The shrinkage curves are shown in Fig. 3a for LSCF2828, LSCF3728 and LSCF5528 and in Fig. 3b for LSCF6428 and LSCF7328. The total shrinkage was in the range of ≈ 11– 16%. The measured relative densities were in the range of ≈ 89– 94% of the theoretical density.

Sintering experiments at a temperature in the range of the second minimum of the shrinkage rate curves ($T_3$) showed that the densification is nearly completed. The shrinkage curves are shown in Fig. 3b for LSCF2828 and LSCF5528 and in Fig. 3c for LSCF3728, LSCF6428 and LSCF7328. As can be seen in the isothermal phase the shrinkage reached an almost constant level after dwelling for 6 h. Here, the total shrinkage was in the range of ≈ 16– 18%. The measured relative sample densities were for all materials higher than 95% of the theoretical value.

Considering a constant sintering temperature it could be stated that the relative shrinkage increases with decreasing lanthanum content in the perovskite lattice. Nevertheless, in case of a sintering temperature of 1050 °C there seems to be an anomaly. Here, the relative shrinkage of LSCF7328 is larger than the relative shrinkage of LSCF6428.

### *3.4. Effect of sintering temperature and sintering dwell time on microstructure and sample density*

The samples were sintered for 0.5–6 h at the above mentioned temperatures. The measured relative sample densities are summarised in Table 4.

In Fig. 4 SEM images of cross-sections of LSCF2828 samples sintered at 1050 °C and 1150 °C for 0.5 h, 3 h and 6 h are shown. As can be seen in the SEM images there were regions which were denser than other regions in case of sintering at 1050 °C for half an hour (Fig. 4a). By increasing the sintering dwell time the relative sample density increased. After 6 h dwelling a relative sample density of about 94% of the theoretical value was achieved (Fig. 4c). Nevertheless, by increasing the sintering temperature to 1150 °C a relative sample density of about 93% of the theoretical density was achieved after 0.5 h sintering. Under this conditions an increase in sintering dwell time seemed to have no effect on the densification of the sample (Fig. 4d–f).

In Fig. 5 SEM images of cross-sections of LSCF3728 samples sintered at 1050 °C and 1250 °C for 0.5 h, 3 h and 6 h are shown. In case of sintering at 1050 °C for 0.5 h there were also regions

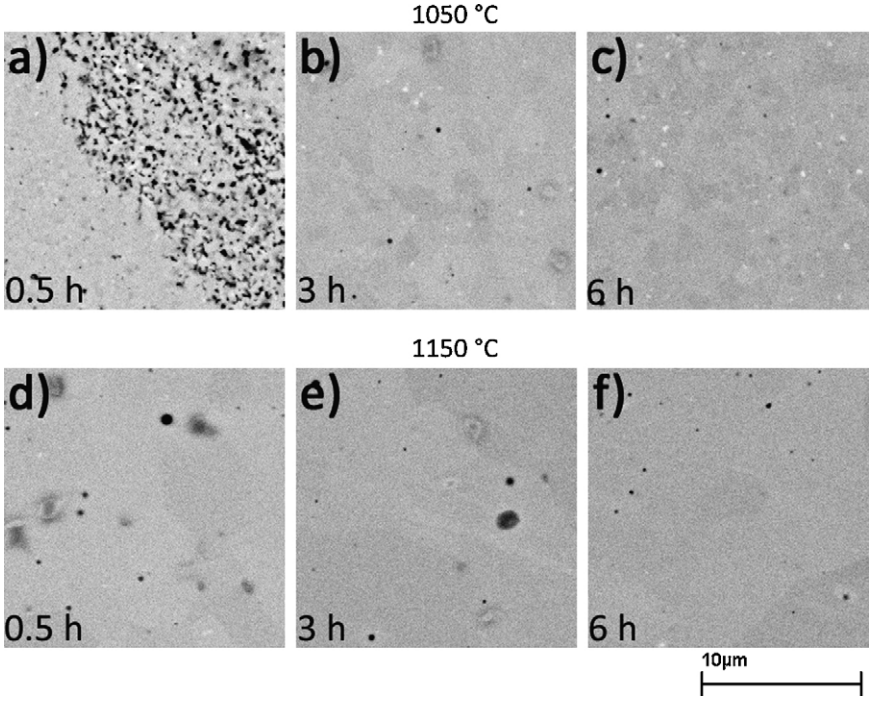


Fig. 4. SEM images of LSCF2828 samples sintered at 1050 °C and 1150 °C.

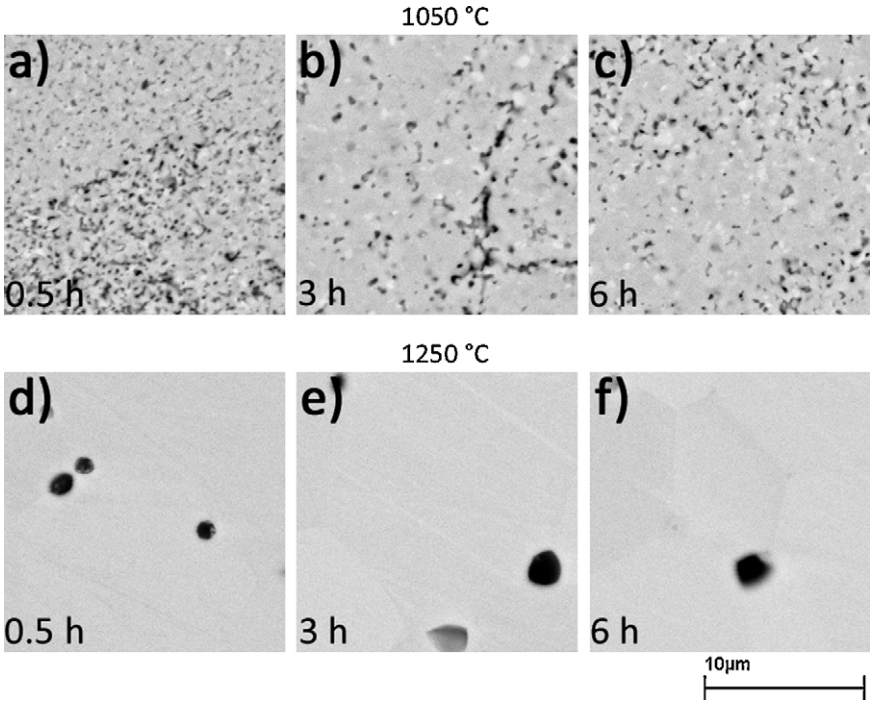


Fig. 5. SEM images of LSCF3728 samples sintered at 1050 °C and 1250 °C.

which were more porous than other regions (Fig. 5a). This was reflected in the measured relative sample density which was about 84% of the theoretical value. The sample became denser by increasing the sintering dwell time. An increase of about 9% occured by increasing the dwell time from 0.5 h to 6 h (Fig. 5a and c). However, by increasing the sintering temperature up to 1250 ° C already after half an hour sintering a relative sample density of more than 95% was achieved (Fig. 5d). Increasing the sintering dwell time at this temperature did not enhance the relative sample density (Fig. 5e–f).

In Fig. 6 SEM images of cross-sections of LSCF5528 samples sintered at 1050 ° C and 1150 ° C for 0.5 h, 3 h and 6 h are shown. Here, also regions which were denser than other regions occured for the sintering experiments at 1050 ° C for 0.5 h and 3 h (Fig. 6a and b). In principle the densification increased with increasing sintering dwell time. Nevertheless, in case of sintering at 1050 °

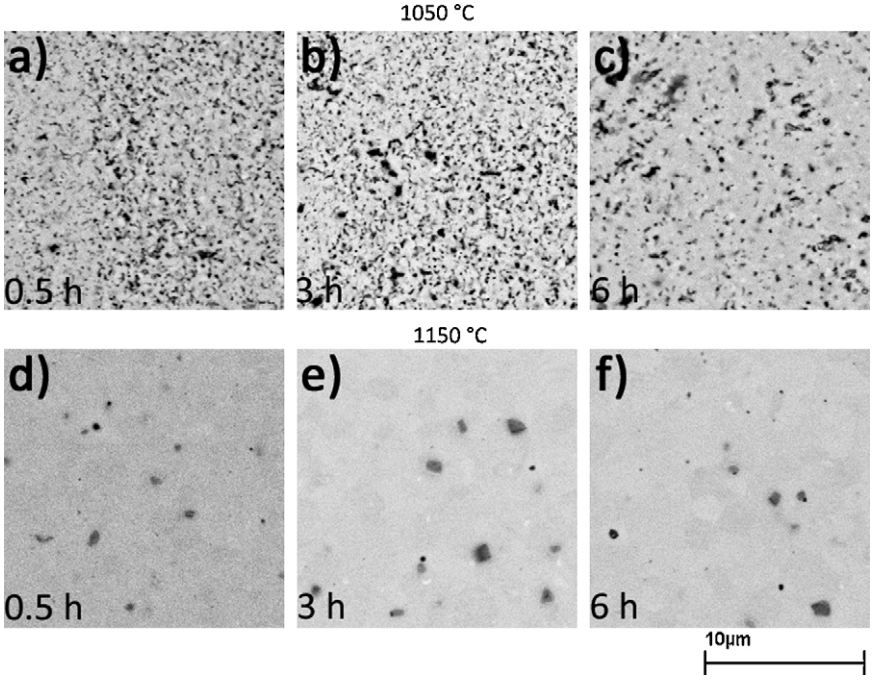


Fig. 6. SEM images of LSCF5528 samples sintered at 1050 °C and 1150 °C.

C for 3 h there was a decrease in relative sample density. Unfortunately, it was not possible to acertain this decrease of relative sample density. However, increasing the sintering temperature to 1150 ° C a relative sample density of almost 94% of the theoretical density could be achieved after 0.5 h dwelling (Fig. 6d). Here, an increase in sintering dwell time seems to have no significant effect on the densification of the sample (Fig. 6d–f).

In Fig. 7 SEM images of cross-sections of LSCF6428 samples sintered at 1050 °C, 1150 ° C and 1250 ° C for 0.5 h, 3 h and 6 h are shown. In case of sintering at the lowest sintering temperature there were for all dwell times regions which were more porous than other regions (Fig. 7a–c). The measured relative sample density was for a dwell time of half an hour comparatively low (61%). Increasing the dwell time should lead to an increase in sample density. However, in case of 6 h dwelling the measured relative sample density decreased strongly. This might be due to cracks in the sample, which occured during green body preparation or the sintering step itself. Increasing the sintering temperature to 1150 ° C the relative sample density increased. Here, no regions occured which are more porous than others (Fig. 7d–f). But, in case of 6 h dwelling again the relative sample density decreased. This also might be due to cracks in the sample. A further increase in sintering temperature (1250 °C) led to a higher densification (87–95%). Here, the increase in dwell time from 3 h to 6 h led to an increase in relative sample density of about 6% (Fig. 7g–i). Unfortunately, there are a few secondary phases (cobalt oxide) formed (e.g. Fig. 7i, marked by a circle). Secondary phases were identified using EDX.

In Fig. 8 SEM images of cross-sections of LSCF7328 samples sintered at 1050 °C, 1150 ° C and 1250 ° C for 0.5 h, 3 h and 6 h are shown. In case of sintering at 1050 ° C the sample was porous even after 6 h dwelling (Fig. 8a–c). The relative sample density increased from 80% to 85% by increasing the dwell time from 0.5 h to 6 h. However, increasing the sintering temperature to 1150 ° C a relative sample density of greater than 94% of the theoretical density was achieved. A further increase in sintering temperature did not lead to a higher densification (Fig. 8g–i). In contrast, by increasing the sintering temperature small spots of secondary phases (cobalt oxide) are formed (Fig. 8h, marked by a circle). Those secondary phases which were also identified using EDX might influence the material properties.

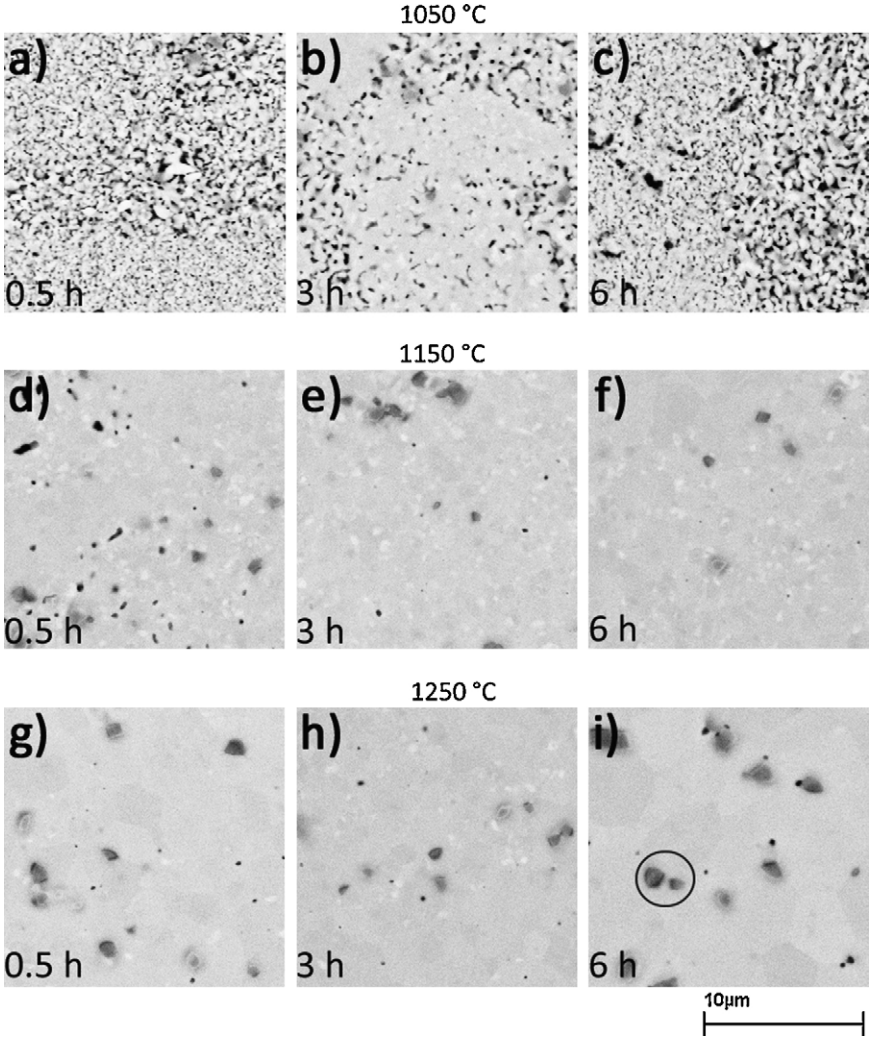


Fig. 7. SEM images of LSCF6428 samples sintered at 1050 °C, 1150 °C and 1250 °C.

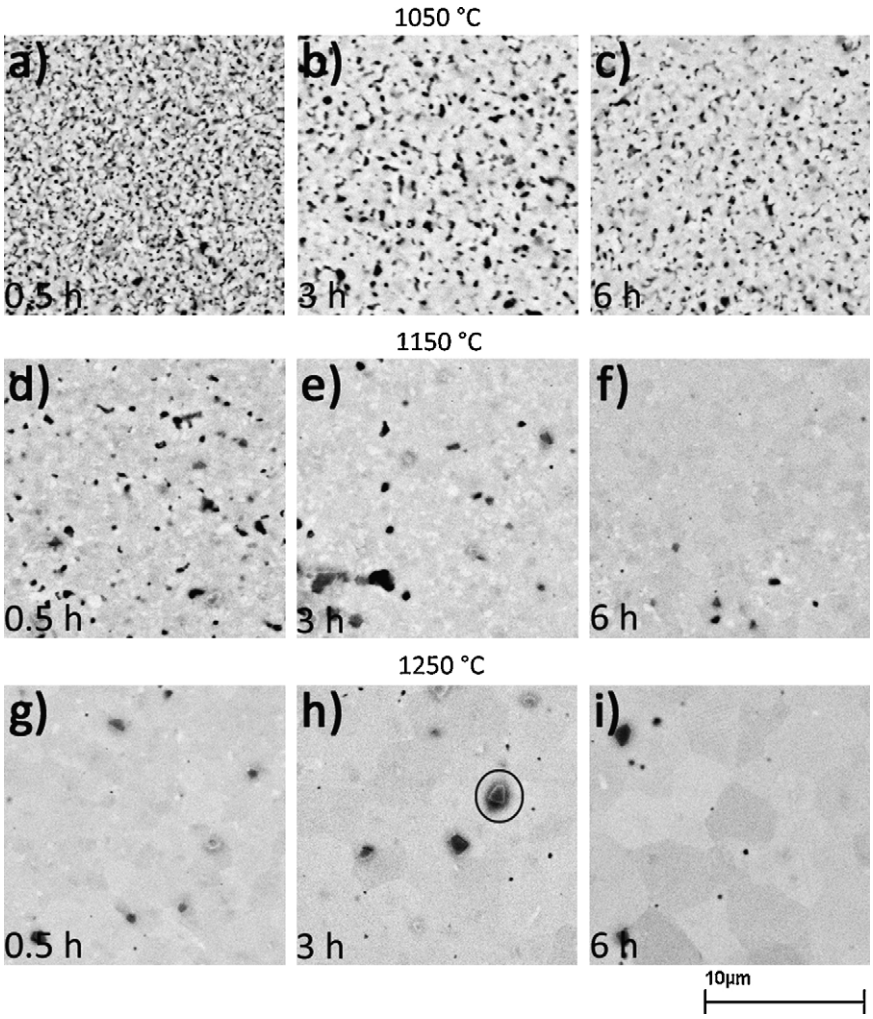


Fig. 8. SEM images of LSCF7328 samples sintered at 1050 °C, 1150 °C and 1250 °C.

In principle it could be stated that the effect of the sintering temperature is more significant than the effect of the sintering dwell time. Increasing the sintering temperature led to a higher densification even at low sintering dwell times for all materials. Considering the lanthanum content of the perovskites, there seems to be no influence of the lanthanum content on the final sintering temperature and dwell time. Nevertheless, only in case of LSCF6428 and LSCF7328 sintering at the temperature in the range of the second minimum of the shrinkage rate curve led to the formation of secondary phases.

## 4. Conclusion

In this study the sintering behaviour of perovskite-type membrane materials within the system $La_{1-x}Sr_xCo_{0.2}Fe_{0.8}O_{3-\delta}$ ($0.3 \leq x \leq 0.8$) was investigated. The perovskite-type materials were prepared by solid state reaction at 1150 ° C for 6–24 h; then ball milled and finally uniaxially pressed into pills.

Shrinkage curves of the samples have been measured using a high-resolution dilatometer. Three different heating rates and three sintering temperatures have been selected to investigate the influence of these parameters on the shrinkage curves and the sample density. The results showed that the influence of the heating rate on the shrinkage curves is negligible in the range of those investigations. Deviations were mostly within the uncertainty of measurement. The total shrinkage of the samples was in all cases less than 25%.

The influence of the sintering temperature was more significant than the influence of the sintering dwell time according to our studies. In case of LSCF6428 and LSCF7328 sintering experiments at the highest temperature which was selected according to shrinkage rate curves showed that secondary phases might occur.

On the basis of our studies it could be stated that the investigation of the sintering behaviour is very important due to the fact that the sintering behaviour is material-dependent.

## Acknowledgements

This work was funded by the German government, Bundesministerium für Wirtschaft und Technologie (BMWi) in the framework of the project OxyMem under the number 0327739B. Furthermore, the authors thank Dr. W. Fischer and M. Ziegner (Forschungszentrum Jülich GmbH, Institute

of Energy Research) for conducting XRD analyses and Dr. E. Wessel (Forschungszentrum Jülich GmbH, Institute of Energy Research) for conducting SEM analyses.

## References

1. Lee, S., Woo, S. K., Lee, K. S. and Kim, D. K., Mechanical properties and structural stability of perovskite-type, oxygen-permeable, dense membranes. *Desalination*, 2006, **193**, 236–243.
2. Arnold, M., Wang, H. and Feldhoff, A., Influence of $CO_2$ on the oxygen permeation performance and the microstructure of perovskite-type $(Ba_{0.5}Sr_{0.5})(Co_{0.8}Fe_{0.2})O_{3-\delta}$ membranes. *Journal of Membrane Science*, 2007, **293**, 44–52.
3. Stevenson, J. W., Armstrong, T. R., Carneim, R. D., Pederson, L. R. and Weber, W. J., Electrochemical properties of mixed conducting perovskites $La_{1-x}M_xCo_{1-y}Fe_yO_{3-\delta}$ (M = Sr, Ba, Ca). *Journal of the Electrochemical Society*, 1996, **143**, 2722–2729.
4. Mosadeghkhah, A., Alaee, M. A. and Mohammadi, T., Effect of sintering temperature and dwell time and pressing pressure on $Ba_{0.5}Sr_{0.5}Co_{0.8}Fe_{0.2}O_{3-\delta}$ perovskite-type membranes. *Materials and Design*, 2007, **28**, 1699–1706.
5. Sagdahl, L. T., Einarsrud, M-A. and Grande, T., Sintering of $LaFeO_3$ ceramics. *Journal of the American Ceramic Society*, 2000, **83**, 2318–2320.
6. Kleveland, K., Einarsrud, M-A. and Grande, T., Sintering behavior, microstructure, and phase composition of $Sr(Fe,Co)O_{3-\delta}$ ceramics. *Journal of the American Ceramic Society*, 2000, **83**, 3158–3164.